Indian Journal of Pure & Applied Physics
Vol. 63, June 2025, pp. 497-507
DOI: 10.56042/ijpap.v63i6.16012

Sequential Phase Feed Based Circularly Polarized RFID Reader Antenna for2.45 GHz Applications

Abhishek Choudhary[1], Deepak Sood[1*] & Priyanka Dalal[2]

[1]Department of Electronics and Communication Engineering, University Institute of Engineering and Technology, Kurukshetra University, Thanesar 136 119, India

[2]Department of Electrical and Electronics Engineering, Guru Jambheshwar University of Science & Technology, Hisar 125 001, India

Received: 26 December 2024; accepted: 19 May 2025

A wideband, circularly polarized (CP) reader antenna is presented for 2.45 GHz RFID systems. To achieve circular polarization, the antenna features a circular radiating patch on the top layer, fed by a sequential phase feed network located on the bottom layer. An air gap is introduced between the two layers to minimize dielectric loss, thereby enhancing directivity and radiation efficiency, which in turn increases overall gain. Cylindrical copper wires passing through the air gap connect the bottom feed network to the top patch layer. By implementing incremental phase variations across the four outputs of the feed network, the antenna achieves a −10 dB impedance bandwidth of 650 MHz (2.02–2.67 GHz) and a circular polarization axial ratio (CP AR) bandwidth of 150 MHz (2.366–2.527 GHz). The antenna exhibits a peak gain of 8.4 dBiC and maintains a symmetric radiation pattern at 2.45 GHz. The physical dimensions of the antenna are 70 × 70 × 13.2 mm³. The design provides a 3 dB axial ratio beamwidth of 91° and a half-power beamwidth of 63.9° in the X–Z plane and 64° in the Y–Z plane. An equivalent circuit analysis is performed to better estimate the antenna's performance. The design is experimentally verified and compared with simulation results. The proposed antenna is particularly suitable for mobile RFID applications operating at 2.45 GHz, such as inventory management, asset tracking, access control, electronic toll collection, and medication distribution.

Keywords: RFID, Reader antenna, Microstrip structure, Sequential phase feed, Circular polarization

Introduction

The RFID technology is experiencing rapid growth and is extensively utilized across various commercial sectors, including supply chain management, logistics control, automatic retail management, e-ticketing, security and access control, transportation, and electronic toll collection[1]. RFID systems, as automatic identification technologies, offer higher recognition accuracy and faster processing compared to traditional methods such as barcodes. International standards for RFID cover different frequency bands: low frequency (LF) at 125–135 kHz (ISO 18000-2), high frequency (HF) at 13.56 MHz (ISO 18000-3), ultra-high frequency (UHF) at 433.92 MHz (ISO 18000-7) and 860–960 MHz (ISO 18000-6), and the industrial, scientific, and medical (ISM) bands at 2.45/5.8 GHz (ISO 18000-4). The 2.45 GHz frequency band is particularly suitable for RFID applications involving miniature items, as it supports the integration of small tag and reader antenna systems.

Additionally, surplus power for tags can be harvested from ambient sources such as Wi-Fi, making it feasible to integrate miniature antennas into smartphones as replacements for traditional readers[2] operating at 2.4 GHz. Consequently, microwave RFID (MW-RFID) systems are increasingly favored in the RFID domain due to their high transmission rates and compact form factors[3]. Recent advancements in RFID technology have led to several proposals for linearly polarized antenna designs specifically intended for RFID readers[4-9]. The antennas referenced in [5,8] demonstrate excellent performance at 2.45 GHz, featuring gains exceeding 9 dB and radiation efficiencies above 85%. However, these antennas are relatively large and exhibit limited −10 dB impedance bandwidths of 120 MHz and 80 MHz, respectively.

In contrast, a smaller-sized design reported in[7] measures (37 × 37 × 5.6) mm³, achieving a 10 dB impedance bandwidth of 130 MHz and a maximum gain of 6.51 dB. Patch antenna arrays have been investigated to enhance radiation characteristics, however, this approach generally results in larger

*Corresponding author: (E-mail: deepaksood.uiet@gmail.com)

overall dimensions[9]. In RFID tag detection, linearly polarized RFID readers experience polarization losses due to tag orientation variability. On the other hand, circularly polarized RFID readers offer increased flexibility by accommodating tags with varying orientations, thereby mitigating the polarization losses.

Therefore, circularly polarized antennas are increasingly adopted to mitigate such issues[10]. Several methods for achieving circular polarization in antennas have been proposed in recent literature[11-22]. Notably, designs [11-19] have demonstrated dual-band functionality. For instance, the design[11] presents an antenna measuring (84×84×1.6) mm^3 but offers limited impedance and axial ratio (AR) bandwidths, achieving a maximum gain of 6.84 dB at 2.45 GHz with 71 percent radiation efficiency. Multiple input multiple output (MIMO) technique[12-13] is employed to achieve high gain but the larger physical dimensions limit their use. In contrast,[14] utilizes a cross-dipole technique to achieve good impedance and AR bandwidths. However, it exhibits a gain of only 3.8 dB at 2.45 GHz. Further, the use of cross dipoles with the artificial magnetic conductor (AMC) [15-16] is used to enhance the gain but exhibits limited bandwidth. The designs reported in[17, 18] address both bandwidth and gain enhancement using an array of cross dipoles along with AMC but at the cost of a larger physical size. Designs[19, 20] offer good axial ratio and gain performance, integrating a dual-feed network comprising a 3 dB wideband Wilkinson power divider and a 90-degree phase shifter. However, these designs involve a complex fabrication process with three substrate layers and lumped elements. Further in the domain of single band operation, the designs reported in [21-22] are compact microstrip antennas offering good impedance bandwidth, with[22] achieving a notable AR bandwidth of 30 percent at 2.45 GHz, albeit with modest gains. Similarly, [23, 24] provide moderate gains exceeding 4 dB but exhibit narrow impedance and AR bandwidths. A helical-shaped[25] antenna offering robust radiation characteristics with a high gain of 8.1 dB and an AR bandwidth of 6.5 percent at 2.45 GHz is reported. The design[26] utilizes an S- shaped impedance matching network and a slotted, corner-truncated radiating patch to get circular polarization, achieving a gain of 6.32 dB, 87 percent radiation efficiency, and 370 MHz impedance bandwidth but exhibits a narrow AR bandwidth resulting increased sensitivity to orientation and poor signal quality.

In this paper, a sequential phase feed network[27] is employed at the bottom layer to achieve circular polarization. The top circular patch is connected to the feed network via cylindrical probes passing through the air gap between two layers. This approach ensures a progressive 90° phase difference across the four output ports of the feed and helps to achieve impedance matching between the network and I/O port, ensuring balanced signal amplitudes across all ports. The proposed antenna is designed to cover the 2.45 GHz band, aiming for optimal performance in terms of impedance matching, AR, and gain characteristics. This work aims to balance the design parameters to simultaneously achieve compactness, high gain, and wideband performance, surpassing many of the already reported designs. Additionally, to get better physical insight discussions on right-hand circular polarization (RHCP), left- hand circular polarization (LHCP), radiation efficiency and equivalent circuit analysis are incorporated. Lastly, a comparison of the proposed design with already reported is provided.

1 Design & Simulation

To achieve high gain, circular polarization, and wideband response, the design process begins with the development of a basic circular patch antenna in stage 1 (H= 0 mm, R =16.67 mm, X = Y= 4mm) on a grounded dielectric substrate, as shown in Fig. 1(a). The radius (R) of the circular patch is calculated using the equations [28] as:

$$R = \frac{F}{\left\{1+\frac{2h}{\pi F \varepsilon_{reff}}\left[ln\left(\frac{\pi F}{2h}\right)+1.7726\right]\right\}^{1/2}} \quad \ldots (1)$$

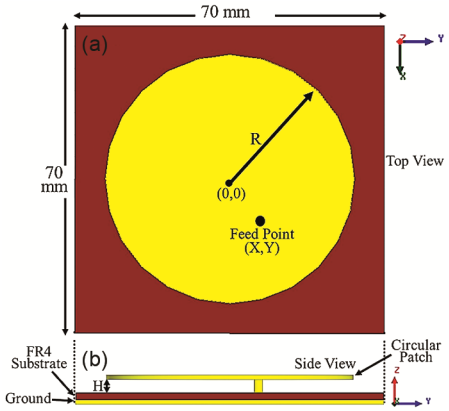

Fig. 1 — Structure of initial stages of antenna (a) Top View, and (b) Side view. Design Stage -1 (H = 0 mm, R = 16.67 mm, X = Y = 4 mm), Design Stage -2 (H = 3 mm, R = 28.15 mm, X = Y = 6.5 mm)

where

$$F = \frac{8.791 \times 10^9}{f_r\sqrt{\varepsilon_{reff}}}, \text{ and } \varepsilon_{reff} \approx 2\frac{\varepsilon_{r1}\varepsilon_{r2}}{(\varepsilon_{r1}+\varepsilon_{r2})} \quad \ldots (2)$$

Here f_r is resonance frequency in Hz, 'h' is the gap between the top circular patch and ground plane (in cm), and ε_{reff} is the dielectric constant of the (FR4 + air) substrate. The simulated S_{11} response, illustrated in Fig. 2, reveals that this initial design demonstrates linear polarization with a -10 dB bandwidth of 58 MHz and a gain of 3.6 dBi. Further, to enhance both gain and bandwidth, in design stage 2 (H= 3 mm, R =28.16 mm, X = Y= 6.5mm) a 3 mm air gap (H) is incorporated[29], as shown in Fig. 1(b). The S_{11} response of this modified design indicates a significant improvement, in -10 dB bandwidth (120 MHz) and a gain of 8.2 dBi. Finally for further enhancement of gain, and bandwidth and to achieve circular polarization an antenna geometry (design stage 3), as depicted in Fig. 3(a), is designed using the circular radiating patch on the top of a substrate (SUB2).

The circular patch is connected to a sequential phase feed network via cylindrical probes of diameter (d) of 2 mm. The phase feed network is designed on a grounded substrate SUB1 which is placed at an air gap (H) of 10 mm below SUB 2 as shown in Fig. 3 (a) and (b). The substrates SUB1 and SUB2 are of FR4 material (ε_r = 4.4 and tanδ = 0.02) and have a thickness (t) of 1.6 mm. The antenna's parametric optimization was conducted using Ansoft HFSS, and optimized dimensions are listed in Table 1. The antenna is centrally fed at port 1 of the feed network. The feed network consists of microstrip lines connecting port 2 to port 4 through port 1 as represented in Fig. 4 (a).

There are two quadrant strip arcs of length $\lambda_g/4$ connecting port 2 to port 3 and port 4 to port 5, as illustrated in Fig. 4(a). Port 2 is positioned at a distance of $\lambda_g/4$ from port 1, providing a 90° phase shift relative to port 1. Port 4 is situated at 3λg/4 from port 1, creating a phase difference of 270° with respect to port 1. Port 3, located $\lambda_g/4$ away from port 2 through the quadrant strip arc introduces a 90° phase shift as illustrated in Fig. 4(a). Similarly, Port 4, located λg/4 away from Port 5 through another quadrant strip arc contributes a 90° phase shift.

The equivalent schematic diagram of the feed network is presented in Fig. 4(b). Consequently, the feed network exhibits sequential phase differences of 0°, 90°, 180°, and 270° across its four ports thereby

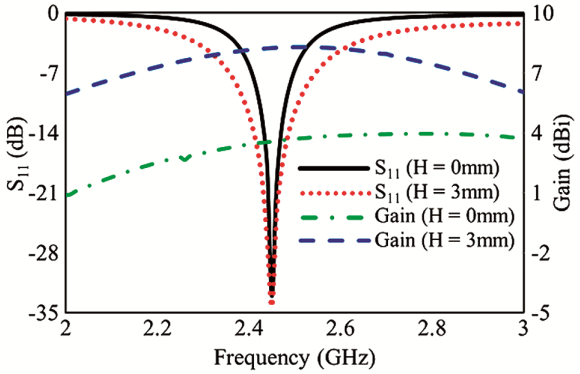

Fig. 2 — Simulated S_{11} and gain responses for design stages 1 and 2

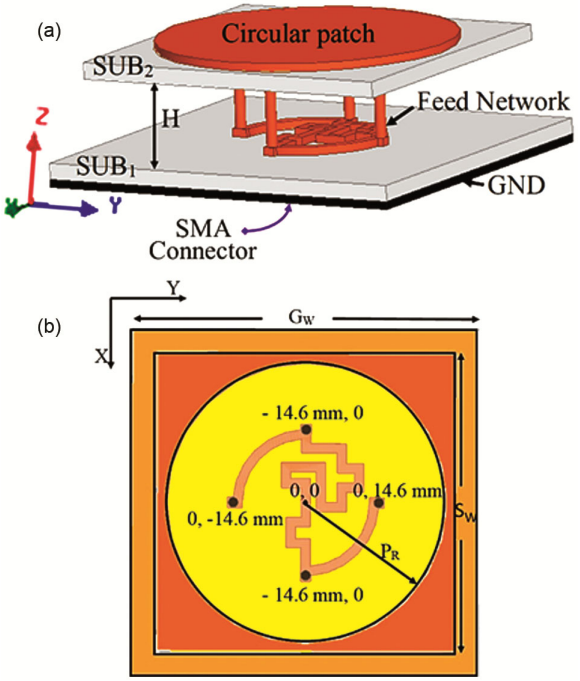

Fig. 3 — The design of proposed antenna. (a) side view of the designed antenna, (b) transparent view of top surface of CP antenna

Table 1 — Optimized Design Parameters of CP Antenna

Parameters	Dimensions in mm	Parameters	Dimensions in mm
L_1	3	S_8	3.5
L_2	6	S_9	5.6
L_3	3	S_{10}	4
L_4	6	S_{11}	7.2
S_1	3	S_{12}	1.9
S_2	4	R	13.7
S_3	5	W	1.8
S_4	8.8	L	70
S_5	8	W	60
S_6	6	H	10
S_7	4	T	1.6

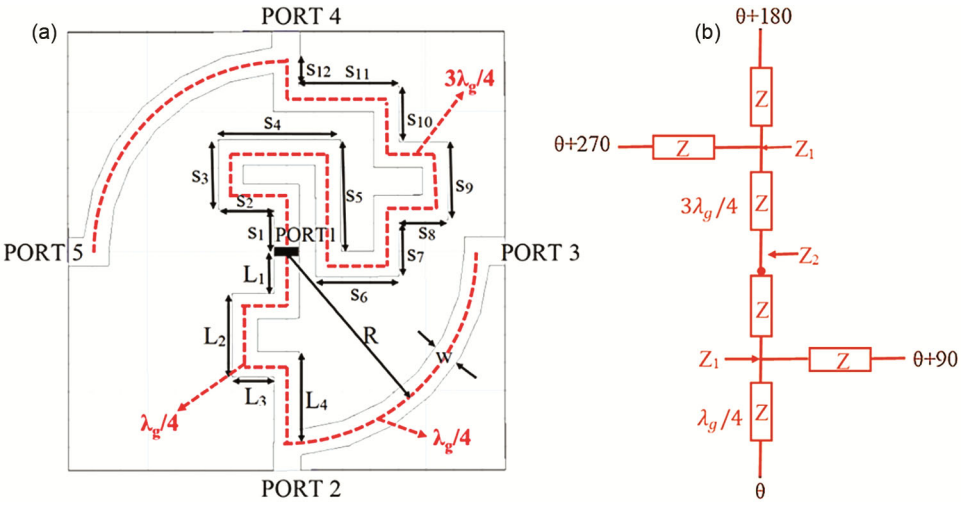

Fig. 4 — The design of proposed antenna (a) dimensions and path length in feed network (b) simplified schematic circuit diagram of feed network.

helping to achieve circular polarization. Sequential phase feeding is one of the famous techniques that can be used to generate circular polarization in a microstrip antenna[27]. This type of feeding leads to significant improvements both in bandwidth and polarization purity. In sequential phase feeding orthogonal feeds are excited at multiple ports with signals that have a controlled phase difference of 90 degree. The impedance and λ_g calculation formulae[30] of the feed network are as:

$$\lambda_g = \frac{v_p}{f} = \frac{c}{f\sqrt{\varepsilon_{eff}}} \quad \ldots (3)$$

$$\text{If } \left(\frac{w}{h} < 1\right) \rightarrow \varepsilon_{eff} = \frac{\varepsilon_r+1}{2} + \frac{\varepsilon_r-1}{2}\left[\frac{1}{\left(1+12\frac{h}{w}\right)} + 0.04\left(1-\frac{w}{h}\right)^2\right] \quad \ldots (4)$$

$$\text{If } \left(\frac{w}{h} \geq 1\right) \rightarrow \varepsilon_{eff} = \frac{\varepsilon_r+1}{2} + \left[\frac{\varepsilon_r-1}{2\left(1+12\frac{h}{w}\right)}\right] \quad \ldots (5)$$

$$\text{If } \left(\frac{w}{h} < 1\right) \rightarrow Z = \frac{60}{\sqrt{\varepsilon_{eff}}} \ln\left[8\left(\frac{h}{w}\right) + 0.25\left(\frac{w}{h}\right)\right] \quad \ldots (6)$$

$$\text{If } \left(\frac{w}{h} \geq 1\right) \rightarrow Z = \frac{120\pi}{\sqrt{\varepsilon_{eff}}} / \left[\frac{w}{h} + 1.393 + 0.667\ln\left(\frac{w}{h} + 1.444\right)\right] \ldots (7)$$

$$Z_1 = Z \parallel Z = Z/2 \quad \ldots (8)$$

$$Z_2 = (Z_1+Z) \parallel (Z_1+Z) = 3\frac{Z}{4} \quad \ldots (9)$$

In Eqs (3) to (7), 'w' denotes the width of the microstrip line in the feeding network, and 'h' represents the height of the substrate. At the center frequency of 2.45 GHz, the effective dielectric constant (ε_{eff}) and the guided wavelength (λ_g) are calculated to be 3.198 and 68.5 mm, respectively. From Eq (9) to ensure that impedance Z_2 equals 50 Ω, the impedance Z must be 66.66 Ω as shown in Fig. 4 (b). Consequently, the width of the microstrip line is calculated as 1.8 mm to achieve an impedance (Z) of 66.66 Ω. The simulation results for the scattering parameters when port 1 is excited are shown in Fig. 5 (a). The scattering parameters S_{21}, S_{31}, S_{41}, and S_{51} are above -10 dB, indicating that the

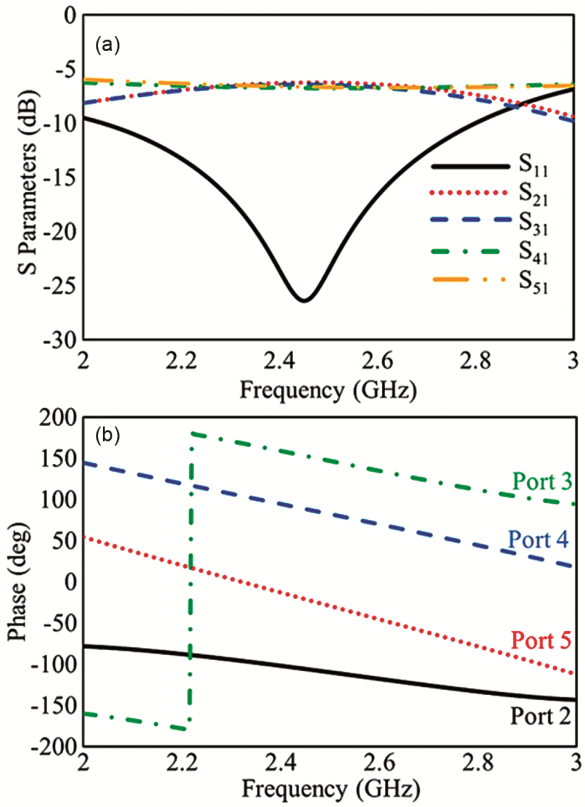

Fig. 5 — (a) Simulated results of the scattering parameters when port-1 is excited., and (b) Simulation of the sequential phase difference of four arms in a feed network

power emitted from port 1 is evenly distributed among all output ports at 2.45 GHz. The S_{11} parameter indicates that the feeding network resonates at the center frequency of 2.45 GHz, with a -10 dB bandwidth spanning from 2.0 to 2.8 GHz. To achieve circular polarization (CP), the electric field vector of the radiated wave is required to rotate in a helical pattern as it propagates away from the antenna. In the proposed design CP is generated by designing a phase feed network in the bottom layer in which a microstrip line-based phase shifter is used to shift the phase of the signals consecutively among four ports in a way that if one port is excited with a signal, the other feed should be excited with a signal that is phase-shifted by 90° relative to the first one. This sequential excitation provides the necessary phase difference for the generation of circular polarization. Figure 5 (b) illustrates the phase differences at the various ports. At 2.45 GHz, the phases at ports 2, 3, 4, and 5 are -109.70°, 160.6°, 82.7°, and -15.2°, respectively. Notably, the phase difference between two consecutive ports is approximately 90°, indicating that the feeding network is capable of generating circularly polarized (CP) radiation when connected to a radiating circular patch.

For further analysis of the impedance characteristics, an equivalent circuit of the complete antenna design has been formed as shown in Fig. 6. In the equivalent circuit, the feed probes are modeled as parallel combinations of four series RL networks. The impedance at the four ports is Z= 66.66 Ω (Fig. 4 (a)) calculated to achieve matching at source port 1 with standard 50Ω.

This impedance 'Z' is inserted in the equivalent circuit as R_f. The 'L_f' represents the inductance of the four cylindrical probes calculated using the Eq (10) as [31]:

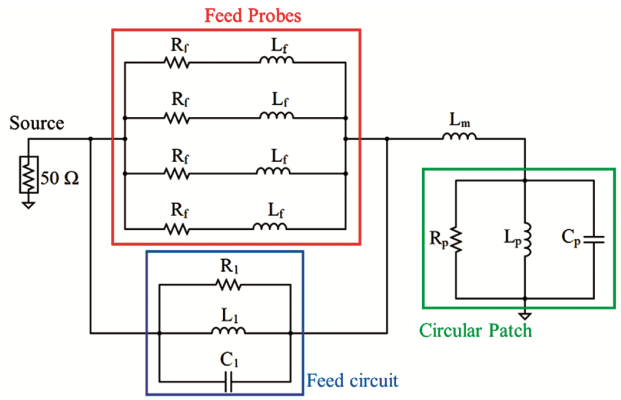

Fig. 6 — Equivalent circuit of the proposed antenna system

$$L_f = 2l\left\{ln\left[\left(\frac{2l}{d}\right)\left(1+\sqrt{1+\left(\frac{d}{2l}\right)^2}\right)\right]-\sqrt{1+\left(\frac{d}{2l}\right)^2}+\frac{\mu}{4}+\left(\frac{d}{2l}\right)\right\}\text{H} \quad \ldots (10)$$

Where 'l ' represents the length of the cylindrical wire in cm, d is the diameter of the wire in cm, μ is the permeability of the copper feed probe is 1.256629×10^{-6} H/m and L_m represents the mutual inductance in between the feed probes. Further, the top circular patch is modeled as a parallel RLC network represented as R_p, L_p, and C_p, which are calculated using the Eqs[32] (11) to (16). As each probe has inductive impedance 'L_f', an air gap embedded between two substrates SUB 1 and SUB 2 is equivalent to a capacitance component 'C_p' to compensate for this inductance[33].

$$R_p = \frac{Q_r}{\omega C_p} \quad \ldots (11)$$

$$L_p = \frac{1}{\omega^2 C_p} \quad \ldots (12)$$

$$C_p = \frac{A\varepsilon_0\varepsilon_{eff}}{h} \quad \ldots (13)$$

$$Q_r = \frac{c\sqrt{\varepsilon_{eff}}}{4fh} \quad \ldots (14)$$

where[34] $\varepsilon_{eff} \approx \frac{\varepsilon_r(h_2+H)}{(h_2+H\varepsilon_r)}$ … (15)

And $h = h_1 + H + h_2$ … (16)

Here, 'A' is the area of the patch, 'h' is the overall height of the design i.e. 13.2 mm, the thickness of the SUB 1 (h_1) and SUB 2 (h_2) are equal to 1.6 mm, and of the air gap (H) is taken as 10 mm, 'ω' is the angular resonance frequency, C_p is the capacitance due to patch and 'Q_r' represents the quality factor. The parallel network of R_1, L_1, and, C_1 represents the effect of the feed circuit on the bottom substrate. The calculated and optimized value of the equivalent circuit are R_f = 66.66Ω, L_f= 5.75 nH, L_m = 0.955 nH, R_p = 52Ω, L_p = 0.618 nH, C_p = 9.84 pF, R_1 = 200 Ω, L_1 = 0.363nH, C_1 =13.44pF. Using these values the impedance of the antenna can be calculated using the Eqs (17) to (20) from the equivalent circuit (Fig. 6) as:

$$Z_A = (Z_f \,||\, Z_1) + j\omega L_m + Z_p \quad \ldots (17)$$

Where

$$Z_f = \frac{R_f + j\omega L_f}{4}, \quad \ldots (18)$$

$$\frac{1}{Z_1} = \frac{1}{R_1} + \frac{1}{j\omega L_1} + j\omega C_1 \quad \ldots (19)$$

$$\frac{1}{Z_p} = \frac{1}{R_p} + \frac{1}{j\omega L_p} + j\omega C_p \quad \ldots (20)$$

The simulated and calculated impedance characteristics are shown in Fig. 7 (a). The calculated real and imaginary values of the impedances follow the simulated values quite closely in the 2.45 GHz RFID band. Similarly, the corresponding simulated and modelled return loss responses are well matched as represented in Fig. 7 (b). In Fig. 8 the current distribution on the radiating circular patch at angles of 0°, 90°, 180°, and 270° is represented. Considering the direction of propagation as +Z, the current rotation depicted in the images demonstrates that the antenna produces a right-hand circular polarization (RHCP) wave.

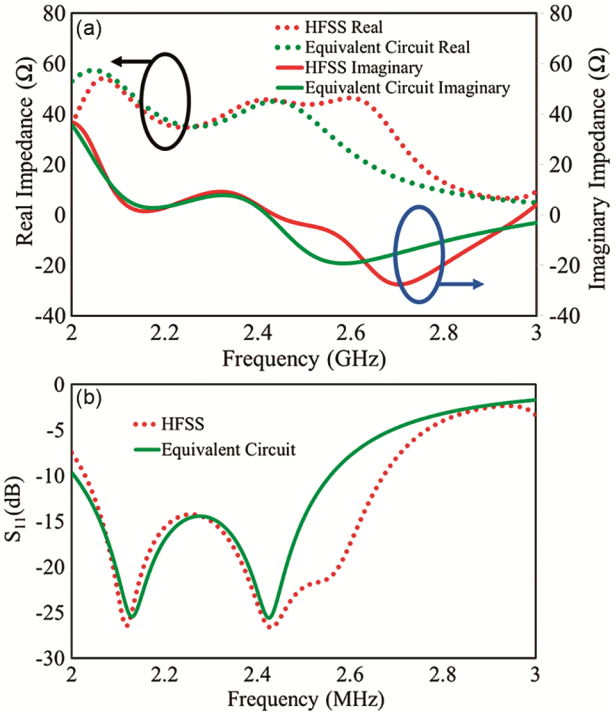

Fig. 7 — Simulated and equivalent circuit based (a) impedance characteristics, and (b) S11 response of the proposed reader antenna

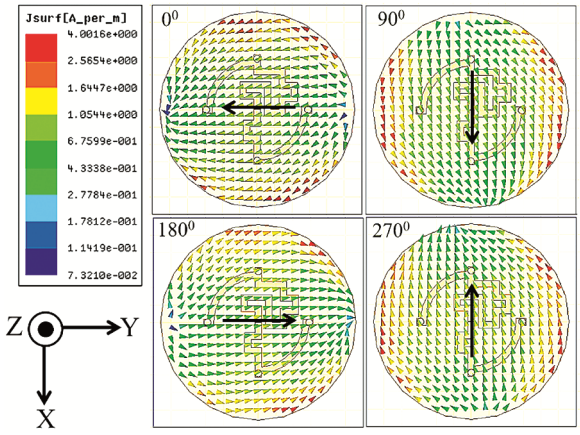

Fig. 8 — Current distribution on the circular patch producing RHCP at 2.45 GHz with different phases: 0°, 90°, 180° and 270°

3 Results & Discussion

All experimental measurements are performed using the vector network analyzer (VNA) of PNA series model N5222A. The fabricated prototype of the proposed circularly polarized antenna is shown in Fig. 9. The comparison of simulated and measured return loss of the designed antenna are shown in Fig. 10 (a). The simulated return loss S_{11} is less than

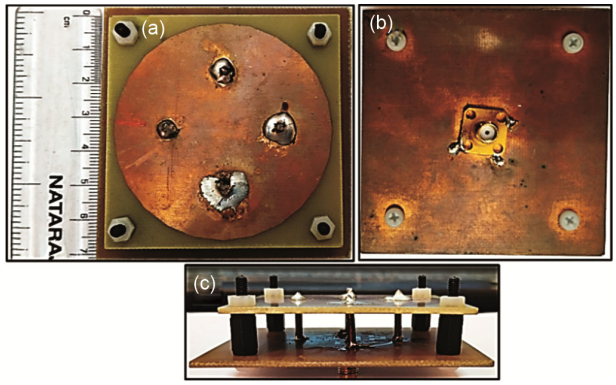

Fig. 9 — The Fabricated prototype of the proposed Circularly polarized antenna for 2.45GHz RFID Applications (a)Top view (b) Bottom view, and (c) Side view

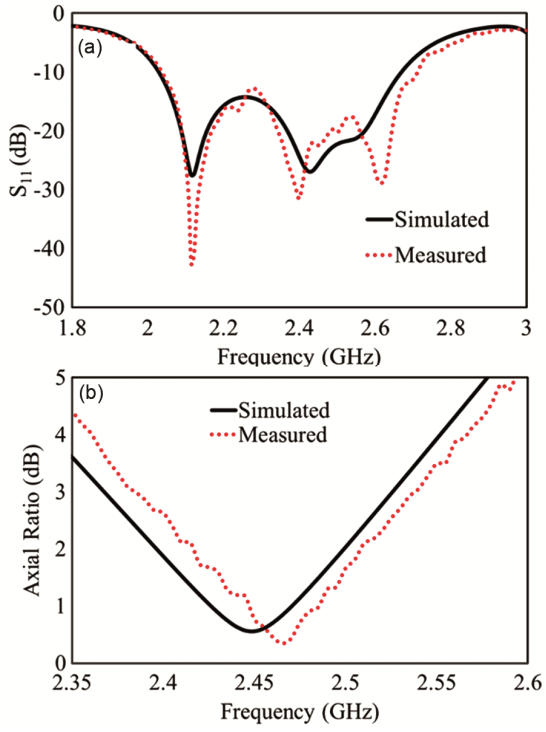

Fig. 10 — Comparison of simulated and measured results of the proposed antenna (a) Return loss, and (b) AR

-10 dB for the frequency range of 2.02GHz to 2.67GHz depicting bandwidth as 27.65%. The measured impedance bandwidth comes out as 28.15 % (2.04 GHz to 2.71 GHz) shown in Fig. 10 (a). The design exhibits 3dB axial ratio (AR) bandwidth from 2.36-2.52 GHz (6.55%) as shown in Fig. 10 (b). For axial ratio measurements S_{21} (dB) is measured with two different orientations (0^0 and 90^0) of antenna for 2.35 GHz to 2.6 GHz. The difference in between two readings is taken as the axial ratio in dB. The measured 3dB AR bandwidth of the antenna is 6.3 % (2.39 to 2.54GHz) as shown in Fig. 10 (b). The measured return loss follows simulated response and, fully covered the 2.40–2.4835 GHz ISM RFID band. Further, small discrepancies between measured and simulated axial ratio is observed as shown in Fig. 10 (b). This may arise due to experimental errors, such as asymmetries from the sub miniature version A (SMA) connector, measurement misalignment, antenna rotation errors, and solder accumulation on the sequential feed probes. The solder lump can act as an unintended inductive or capacitive element, causing amplitude and phase imbalances, distortion in current distribution, and field asymmetry ultimately degrading polarization purity and shifting the axial ratio minimum.

Further, the antenna gain is experimentally measured using three antenna gain measurement system[33,34] by positioning, the fabricated prototype from a reference horn antenna at a distance sufficient to ensure that near-field effects do not impact the far-field measurements as illustrated in Fig. 11. The far-field distance is calculated using the formula $2D^2\backslash\lambda$, where 'D' represents the antenna's largest dimensions and 'λ' denotes the operating wavelength. For gain measurements initially, two UWB horn antennae (ant 1 and ant 2) are positioned in front of each other at above far field distance, and transmission parameters (S_{21} (ant1, ant2)) are measured as illustrated in Fig. 11 (a). In the second step horn antenna (ant 1) is replaced with the fabricated prototype (DUT) and transmission parameters (S_{21} (DUT, ant1)) are measured. Thereafter, ant 2 is replaced with ant 1 again and transmission parameters (S_{21} (DUT, ant2)) are measured as shown in Fig. 11(b). Finally, the gain is calculated through Eq (21) following comprehensive derivation of the gain measurement methodology detailed in[36].

$$G_{DUT} = \frac{\left(S_{21(DUT,ant1)} + S_{21(DUT,ant2)} - S_{21(ant1,ant2)} - L_f\right)}{2} \quad \ldots (21)$$

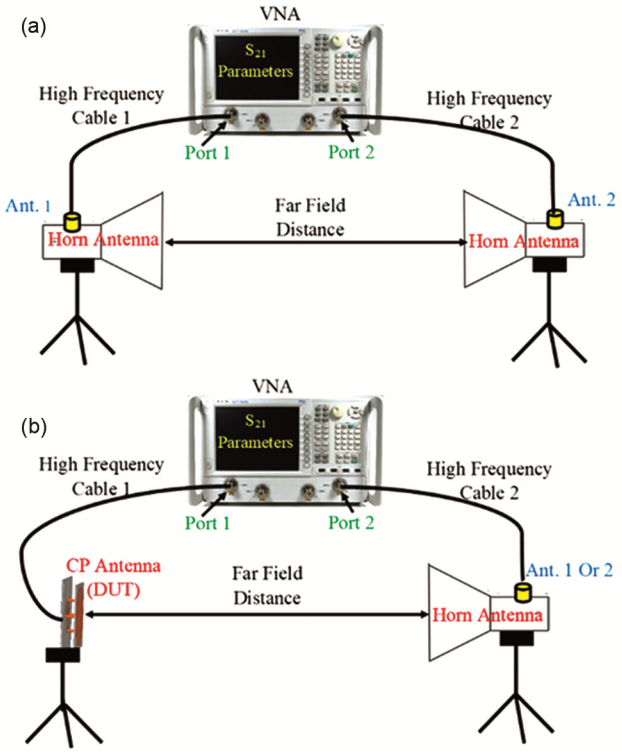

Fig. 11 — Setup for gain measurement using three antenna with unknown gain characteristics (a) Measurement setup for measuring S_{21} parameters between Ant 1 and Ant 2, and (b) Measurement setup for measuring S_{21} parameters between circularly polarized proposed antenna (DUT) and Ant 1 or Ant 2

where L_f is the free space path loss at 2.45 GHz at a distance 1.8 m.

The measured gain exceeds 8 dBic throughout the ISM RFID band, reaching a peak of 8.4 dBic at 2.45 GHz, as shown in Fig. 12. Both simulated and measured results confirm that the designed reader antenna maintains a gain above 8 dBic across the band, with the simulated peak gain being 8.24 dBic at 2.45 GHz.

The antenna radiation pattern at the center frequency of 2.45 GHz is shown in Fig. 13. The radiation pattern is measured by rotating the proposed antenna in both the XZ ($\phi = 0°$) and YZ ($\phi = 90°$) plane in front of the reference horn antenna. In both planes, symmetrical patterns and wide-angle AR characteristics have been observed. The simulated front-to-back ratio at 2.45GHz is 19.6 dB. The simulated and measured RHCP and LHCP of the proposed antenna in the X-Z and Y-Z planes at 2.45 GHz are shown in Fig. 13 (a) and (b), respectively. The simulated and measured values of 3dB half-power beamwidth (HPBW) at 2.45GHz are summarized in Table 2.

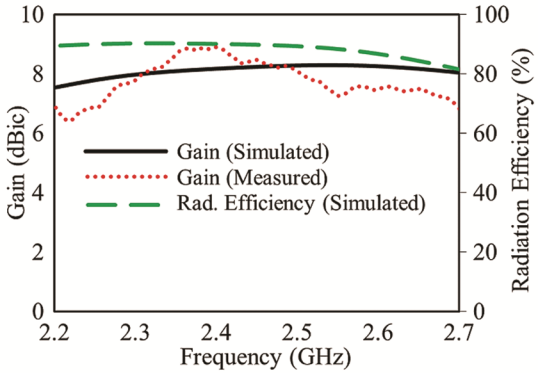

Fig. 12 — Gain and radiation efficiency of the proposed antenna

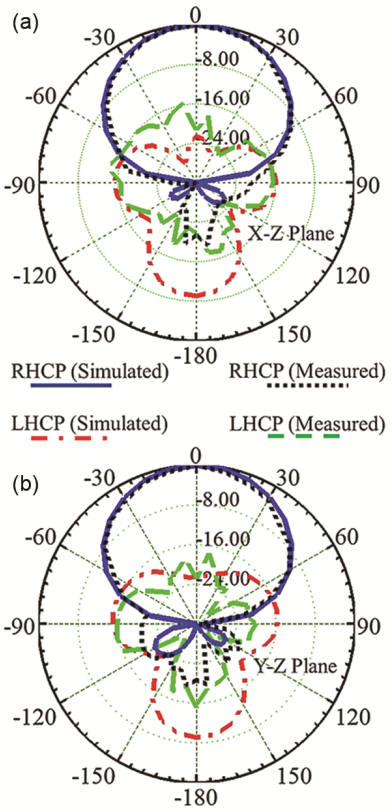

Fig. 13 — Simulated and measured RHCP and LHCP at 2.45 GHz for the proposed antenna (a) X-Z Plane, and (b) Y-Z plane

Table 2 — Half-power beam width performance

Results	X-Z Plane ($\phi = 0^0$)	Y-Z Plane ($\phi = 90^0$)
Simulated	63.9° (-31.5^0 to 32.4^0)	64° (-31.7^0 to 32.3^0)
Measured	59.1° (-28.4^0 to 30.7^0)	56.7° (-28^0 to 28.7^0)

The designed antenna produces RHCP mode towards the +Z direction. The polarization isolation at the broadside direction is greater than

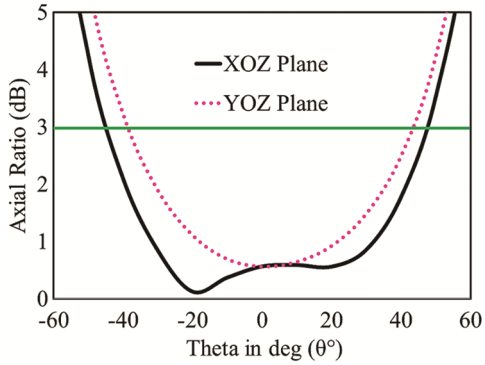

Fig. 14 — Axial Ratio beam width for varying 'θ' in X-Z ('ϕ' = 0°) and Y-Z ('ϕ' = 90°) plane

15 dB in both the X-Z and Y-Z planes indicating a good cross-polarization rejection. In addition to this, the antenna exhibits a high front-to-back ratio greater than 19 dB across the operating bandwidth. Figure 14 represents the AR beamwidth in both X-Z and Y-Z planes. The designed antenna exhibits a simulated 3dB AR beamwidth of 91.17° (-44.23°, 46.94°) in the X-Z plane, 81.2° (-38.3°, 42.9°) in the Y-Z plane, and the minimum AR value at the boresight is 0.5 dB at the center frequency.

The impact of ground plane size (L) on the performance of the designed antenna is analyzed in Fig. 15. As depicted in Fig. 15 (a), the impedance bandwidth remains largely unaffected by variations in ground plane size. However, an increase in 'L' from 60 mm to 65 mm results in a leftward shift in the operating frequency range and a reduction in the axial ratio, indicating an improvement as shown in Fig. 15 (b). A larger ground plane facilitates a more uniform radiation pattern and reduces surface waves, enhancing the axial ratio, impedance bandwidth, and gain. Nevertheless, further increase in the ground plane size can deteriorate the axial ratio and gain as beyond a certain size, the edge diffraction, scattering, higher-order modes, and parasitic effects are increased. Consequently, the ground plane size for the optimized antenna is set to 70 mm, achieving an impedance bandwidth of 640 MHz (-10 dB, from 2.03 to 2.67 GHz), an axial ratio of 0.5 dB, gain of 8.3 dBic and FBR is 19.5 dBi at 2.45 GHz as illustrated in Fig. 15 (a-d).

As shown in Fig. 16 (a), the diameter of the feeding probe has minimal impact on impedance matching as a small variation in impedance bandwidth has been observed. However, an increase in 'H' enhances the

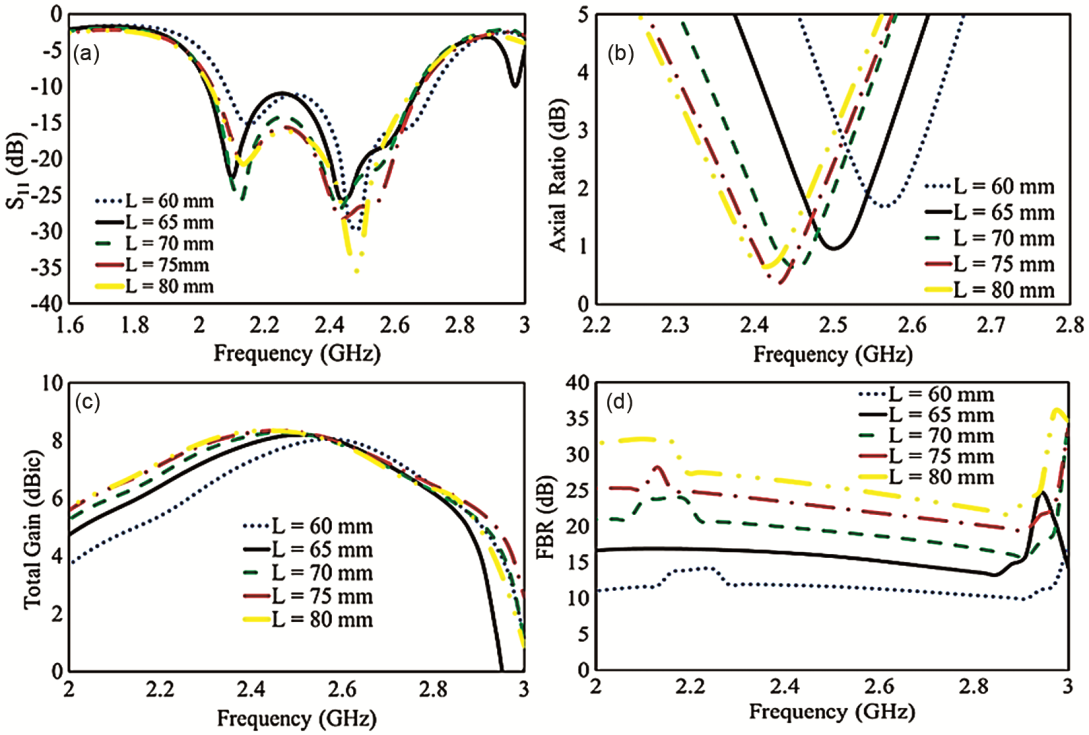

Fig. 15 — Effect of the size of the ground plane L on the performance of the antenna. (a) Return loss (b) AR (c) Gain, and (d) FBR

axial ratio's magnitude but results in a leftward shift in frequency, indicating a change in phase characteristics. A long, thin probe increases inductance, which can disrupt the feed point's phase characteristics and affect axial ratio performance, as illustrated in Fig. 16 (b) and Fig. 17 (b). Based on this analysis, the probe diameter should be between 2 mm and 2.5 mm. The optimized probe diameter is chosen as 2 mm, with a corresponding probe height of 10 mm to achieve an impedance bandwidth of 640 MHz and an axial ratio of 0.5 dB at 2.45 GHz, as depicted in Fig. 16 (a) and Fig. 17 (b).

In Table 3 a comparative analysis of various antennas in terms of polarization, size, impedance bandwidth, 3-dB axial ratio (AR) bandwidth, and peak gain is presented. The comparison indicates that the proposed antenna demonstrates better performance in gain, impedance bandwidth, and 3-dB AR bandwidth within the 2.45 GHz band while maintaining a compact form factor. Antennas described in[5-9] operate in linear polarization mode and experience polarization losses. Although antennas[5,9] exhibit higher gain compared to the proposed design, they are significantly larger and offer narrower impedance bandwidths. In contrast, designs reported in references[11-20] utilize circular polarization and exhibit dual-band characteristics. Another approach[13]

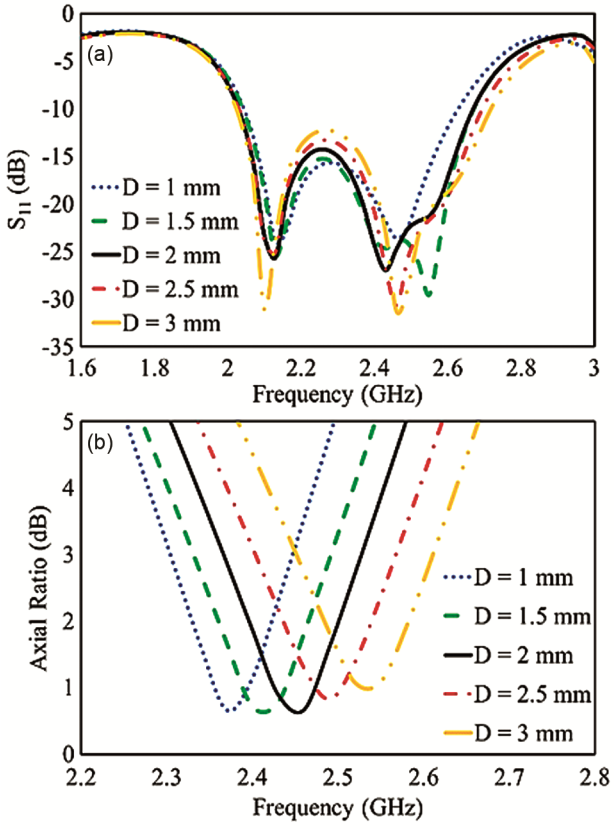

Fig. 16 — Effect of diameter (D) of feeding probe on the performance of antenna (a) Return loss, and (b) AR

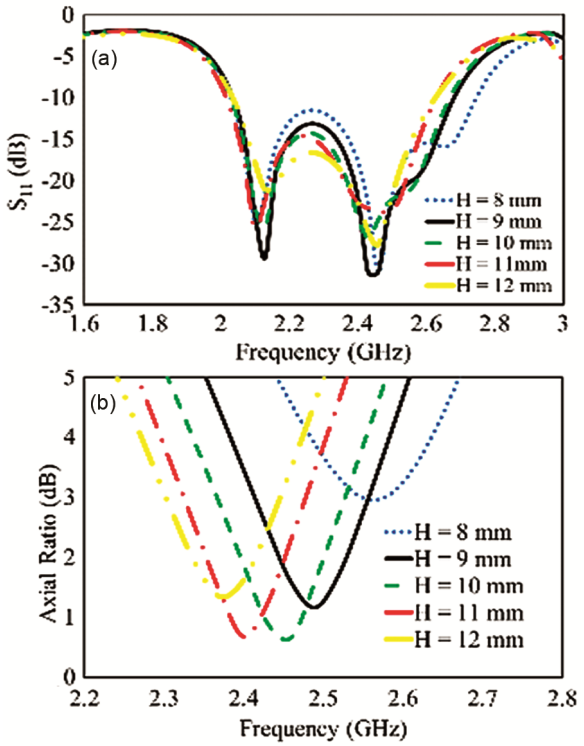

Fig. 17 — Effect of height (H) of feeding probe on the performance of antenna (a) Return loss, and (b) AR

incorporated the three layers structure which is a combination of aperture coupled feed network, patch, and meta surface which makes the antenna large and also the performance of the antenna is less as compared to the proposed antenna. Notably, reference[14] employs a cross-dipole configuration that provides improved impedance and AR bandwidth compared to the proposed antenna; however, it achieves a gain of only 3.8 dBic. To enhance gain[15,16] incorporate a cross-dipole configuration with arrays of artificial magnetic conductors (AMCs), which facilitates unidirectional radiation. While this approach increases the antenna's size, it results in reduced impedance and a narrower 3dB axial ratio bandwidth. Consequently, the gain of these antennas remains lower compared to the proposed antenna. Further, designs[17,18] integrate arrays of antennas with AMCs, although this also leads to an increase in antenna size. Designs[19,20] achieve substantial AR bandwidth, but design[20] presents a smaller impedance bandwidth and larger overall size compared to the proposed antenna. Compact coplanar microstrip patch antennas reported[21,22] offer good impedance and AR bandwidth. The[22] achieves a notable 30% AR

Table 3 — Performance comparison with published work

Ref.	Pol.	Size (mm^3)	Total Size (λ)	Impedance BW	AR BW (%)	Gain (dBi)
[5]	LP	150×150×7.574	1.22×1.22×0.06	120 MHz	-	9.56
[6]	LP	65×60 mm^2	0.53×0.489	-	-	2.03
[7]	LP	37×37×5.6	0.3×0.3×0.045	130 MHz	-	6.51
[8]	LP	190×190×7.635	1.55×1.55×0.062	80 MHz	-	9.4
[9]	LP	227×95.9×1.6	1.85×0.78×0.013	95 MHz	-	7.75
[11]	CP	84×84×1.6	0.68×0.68×0.013	47 MHz	1.5	6.84
[12]	CP	119×119×13	0.97×0.97×0.106	310 MHz	3.5	7.3
[13]	CP	240×240×34	1.96×1.96×0.277	300 MHz	9.6	7
[14]	CP	85×85×1.6	0.694×0.694×0.013	640 MHz	9.3	3.8
[15]	CP	72×72×8.2	0.59×0.59×0.067	250 MHz	4.0	6.1
[16]	CP	112×112×8.2	0.915×0.915×0.18	160 MHz	1.64	6.25
[17]	CP	255×255×39.5	2.08×2.08×0.322	1050 MHz	27.8	15
[18]	CP	270×270×40.62	2.2×2.2×0.331	1000 MHz	23.9	13.3
[19]	CP	150×150×10.36	1.22×1.22×0.084	950 MHz	21.5	8.2
[20]	CP	104×104×6.6	0.85×0.85×0.05	350 MHz	22.3	8.9
[21]	CP	52×52×1	0.42×0.42×0.008	1040 MHz	25.8	3.8
[22]	CP	60×60×1.5	0.49×0.49×0.012	1100 MHz	30	¡3
[23]	CP	40×40×1.6	0.32×0.32×0.013	154 MHz	-	5.32
[24]	CP	30×30×1.6	0.25×0.25×0.013	80 MHz	0.85	4.1
[25]	CP	Dia = 80.8 mm, H = 18.36 mm	Dia = 0.66λ, H = 0.15λ	-	6.5	8.1
[26]	CP	58×58×11	0.47×0.47×0.089	370 MHz	3.25	6.32
[35]	CP	65×65×11.27	0.52×0.52×0.09	400 MHz	3.69	6
Proposed Design	CP	70×70×13.2	0.57×0.57×0.10	650 MHz	6.56	8.24

bandwidth at 2.45 GHz; however, its gain is significantly lower than that of the proposed antenna. The designs[23,24] utilize truncation and miniaturization techniques with circular polarization for size reduction, achieving moderate gains exceeding 4 dB but exhibiting narrow impedance and AR bandwidths. The helical-shaped antenna design[25] shows comparable gain and AR bandwidth to the proposed antenna, but lacks experimental validation. Finally, the designs[26,35] employ slotted patches and air gaps to enhance gain and achieve circular polarization. Despite these modifications, their impedance bandwidth, AR bandwidth, and gain fall short of the proposed antenna's performance. Overall, the proposed antenna is distinguished by its compact size, ease of fabrication, and superior impedance and AR bandwidth, coupled with excellent gain relative to most other designs in the literature.

4 Conclusion

This paper presents the design of a circularly polarized antenna operating at 2.45 GHz. The antenna features a sequential phase feed structure and a circular radiating patch. The radiating patch is sequentially fed through cylindrical probes and an air gap is introduced between the top and bottom layers to achieve high gain and circular polarization. Despite its compact dimensions of (70 × 70 × 13.2) mm3, the antenna experimentally demonstrates a 10 dB impedance bandwidth spanning from (2.04 to 2.71) GHz (28.15%), a 3 dB axial ratio (AR) bandwidth from 2.39 GHz to 2.54 GHz (6.3%) and radiation efficiency is nearly 90%. The maximum gain exceeds 8 dBic across the entire ISM RFID frequency band with a peak value of 8.4 dBic at 2.45 GHz. The antenna exhibits stable symmetrical RHCP radiation patterns with a wide-angle half-power beamwidth of 63.9° in X-Z plane and 64° in Y-Z plane making it ideal for unidirectional, wide-angle RFID applications. This circularly polarized antenna is well suited for RFID and other wireless applications such as IOT integrated with Wi-Fi.

References

1 Wu D L, Ng W W Y, Yeung D S, *et al.*, IEEE Int Conf Machine Learning and Cybernetics, Baoding, China, (2009) 2330.
2 Hande A, Bridgelall R & Bhatia D, Energy harvesting technologies, Springer, Boston, MA, (2009).
3 Paret D, RFID at Ultra and Super High Frequencies: Theory and Application, *Wiley*, (2010).
4 Fan Z G, Qiao S, Huangfu J T, *et al.*, *Prog Electromagn Res*, 71 (2007) 149–158.
5 Mobashsher A T, Islam M T & Misran N, *IEEE Antennas Wirel Propag Lett*, 9 (2010) 653.
6 Singh R K, Michel A, Nepa P, *et al.*, *IEEE J Radio Freq Identif*, 4 (4) (2020) 420.
7 Yang H, Yan S, Chen L, *et al.*, IEEE ISECS Int. Colloquium Comput Commun Control Manage, Guangzhou, China, (2008) 505.
8 Sabran M I, Rahim S K A, Abdul Rahman A Y, *et al.*, IEEE Antennas Wirel Propag Lett, 10 (2011) 979–982.
9 Tabakh I, Das S, Jorio M, *et al.*, Int J Microw Opt Technol, 15 (2020) 517.
10 Gao S, Luo Q & Zhu F, Circularly Polarized Antennas, Wiley, Hoboken, NJ, USA, (2014).
11 Sarkar S & Gupta B, IEEE Int. Conf. RFID Technol Appl (RFID-TA), Pisa, Italy, (2019) 448.
12 Zhang E, Michel A, Nepa P, *et al.*, *Int J Antennas Propag*, (2021).
13 Doan T N H, Nguyen K K, Ta S X, *IEEE Access*, 12 (2024) 78833.
14 Lai F P, Yang J F, Chen Y S, *IEEE Antennas Wirel Propag Lett*, 19 (8) (2020) 1429.
15 Bajaj C, Upadhyay D K, Kumar S, *et al.*, *IEEE J Radio Freq Identif*, 8 (2024) 88.
16 Bajaj C, Upadhyay D K, Kumar S, *et al.*, IEEE Trans Antennas Propag, 72(2) (2024) 1929–1934.
17 Xu R, *et al.*, *IEEE Trans Antennas Propag*, 69 (12) (2021) 8194.
18 Xu R & Shen Z, *IEEE Trans Antennas Propag*, 71(12) (2023) 9593.
19 Liu Q, Shen J, Liu H, *et al*., *IEEE Trans Antennas Propag*, 62 (12) (2014) 6428.
20 Liu Q, Shen J, Liu H, *et al.*, *IEEE Trans Antennas Propag*, 62 (12) (2014) 6428.
21 Chen L, Ren X, Yin Y, *et al*., Prog Electromagn Res Lett, 41 (2013) 77.
22 Birwal A, Kaushal V & Patel K, *IEEE J Radio Freq Identif*, 6 (2022) 593.
23 Luzon M A, Gerasta O J, IEEE Int. Conf. HNICEM, Baguio City, Philippines, (2018) 1–6.
24 Gautam A K, Farhan M, Agrawal N, *et al.*, *IET Microw Antennas Propag*, 13 (13) (2019) 2310.
25 Zainud-Deen S H, Badaway M M, Malhat H A, *et al*., IEEE Nat. Radio Sci Conf (NRSC), Cairo, Egypt, (2014) 1–8.
26 Wu T, Su H, Gan L, *et al.*, *IEEE Antennas Wirel Propag Lett*, 12 (2013) 623.
27 Rasekhmanesh M H, Piroutiniya A & Mohammadi P, *Microw Opt Lett*, 59 (2017) 2806.
28 Balanis C A, Antenna Theory: Analysis and Design (3rd ed.), Wiley, Hoboken, NJ, USA, (2005).
29 Ozenc K, Aydemir M E & Öncü A, IEEE Int. Conf. Recent Adv Space Technol (RAST), Istanbul, Turkey, (2013) 499.
30 Gupta K C, Garg R & Bahl I J, Microstrip Lines and Slotlines (2nd ed.), Artech House, Dedham, MA, USA, (1996) 102.
31 Grover F W, Inductance Calculations: Working Formulas and Tables, Dover Publications, New York, NY, USA, (1946).
32 Mishra P, Mohan A & Ray P, *Int J Appl Electromagn Mech*, 47 (1) (2015) 163.
33 Lin C, Zhang F S, Jiao Y C, *et al*., *IEEE Antennas Wirel Propag Lett*, 9 (2010) 359.
34 Abboud F, Damiano J P & Papiernik A, *IEEE Trans Antennas Propag*, 38 (11) (1990) 1882.
35 Birwal A, Patel K & Singh S, *IEEE J Radio Freq Identif*, 8 (2024) 10.
36 Gao K, Liu H, Liu L, *et al*., IEEE Int. Conf. Sens Meas Data Analytics AI (ICSMD), Xi'an, China, (2020) 557.